Title

Comparison of Ferumoxytol-enhanced MR Angiography and CT Angiography for the Detection of Pulmonary Arteriovenous Malformations in Hereditary Hemorrhagic Telangiectasia: Initial Results.

Journal

Radiology. Cardiothoracic imaging, 2(2)

ISSN

2638-6135

Authors

Khan, Sarah N
McWilliams, Justin P
Bista, Biraj B
et al.

Publication Date

2020-04-01

DOI

10.1148/ryct.2020190077

Peer reviewed

Radiology: Cardiothoracic Imaging

ORIGINAL RESEARCH

Comparison of Ferumoxytol-enhanced MR Angiography and CT Angiography for the Detection of Pulmonary Arteriovenous Malformations in Hereditary Hemorrhagic Telangiectasia: Initial Results

Sarah N. Khan, MD • *Justin P. McWilliams, MD* • *Biraj B. Bista, MD* • *Stephen Kee, MD* • *J. Paul Finn, MD*

From the Department of Radiological Sciences, University of California at Los Angeles, Peter V. Ueberroth Building Suite 3371, 10945 Le Conte Ave, Los Angeles, CA 90095-7206. Received May 23, 2019; revision requested June 20; revision received October 29; accepted October 31. **Address correspondence to** J.P.F. (e-mail: *pfinn@mednet.ucla.edu*).

Work supported by funding from the UCLA Radiological Sciences Exploratory Research Program.

Conflicts of interest are listed at the end of this article.

Radiology: Cardiothoracic Imaging 2020; 2(2):e190077 • https://doi.org/10.1148/ryct.2020190077 • Content code: CH

Purpose: To perform a preliminary comparison of the sensitivity and positive predictive value of ferumoxytol-enhanced MR angiography with those of CT angiography for detection of pulmonary arteriovenous malformations (AVMs) in hereditary hemorrhagic telangiectasia (HHT).

Materials and Methods: Institutional review board approval and informed patient consent were obtained. Ten patients with pulmonary AVMs who had undergone CT of the chest within 12 months underwent MRI of the chest and abdomen with ferumoxytol at 3.0 T at a dose of 4 mg per kilogram of body weight. Consensus review of MR and CT images assessed the presence and characteristics of pulmonary AVMs, image quality, vessel visibility, and artifact grade.

Results: Forty-three AVMs were detected, 13 native and 30 recanalized. Twenty-one AVMs had a feeding artery diameter of greater than 2 mm, of which detection occurred in 19 (at MRI and CT), in two (at MRI only), and zero (at CT only). Twenty-two AVMs had a feeding artery diameter of less than or equal to 2 mm, of which detection occurred in 16 (at MRI and CT), six (at CT only), and zero (at MRI only). For the entire cohort, the sensitivity of ferumoxytol-enhanced MRI using CT as the reference standard was 85.4% (35 of 41), and the positive predictive value was 100% (35 of 35). No significant difference was found between CT and MRI in AVM size, feeding artery and draining vein diameter, and artifact score ($P > .05$ for all).

Conclusion: Initial results suggest that ferumoxytol-enhanced MRI is a feasible alternative to CT for detection of pulmonary AVM in HHT, while avoiding repeated exposure to radiation, nephrotoxic contrast material, or gadolinium-based contrast agent.

Hereditary hemorrhagic telangiectasia (HHT) manifests with multiple arteriovenous malformations (AVMs) in the skin, mucous membranes, spine, brain, liver, gastrointestinal tract, pancreas, and lungs. The disease has an autosomal dominant inheritance and affects one in 5000 individuals (1–5). Bleeding is a common consequence of the presence of AVMs, and many patients with HHT also have coexisting iron deficiency anemia.

Pulmonary AVMs occur in 15%–50% of patients with HHT (6), with clinical complications that include fatal hemoptysis, hemothorax, stroke, and cerebral abscess (7). The rationale for screening for AVMs is to detect a treatable lesion prior to the development of a complication. International guidelines currently recommend transthoracic echocardiography or CT for pulmonary AVM screening (4).

Contrast material–enhanced MR angiography may play an important role in screening for vascular malformations. The advantages of contrast-enhanced MR angiography include visualization of the entire body vasculature in one examination, evaluation of arterial and venous phases in the same study, lack of ionizing radiation, and ease of multiplanar reconstruction.

The safety of gadolinium-based contrast agents (GBCAs) at MRI has been coming under increasingly close scrutiny because of concerns about nephrogenic systemic fibrosis and gadolinium retention in the brain. No gadolinium-based blood pool agents are currently available today.

Ferumoxytol is the focus of growing interest for vascular MRI applications (8–12). Initially developed as a vascular MRI contrast agent, ferumoxytol does not contain gadolinium; rather, it is an iron-based nanoparticle that has been approved by the U.S. Food and Drug Administration as a therapeutic agent for iron deficiency anemia since 2009 (11). However, the magnetic and pharmacokinetic properties of ferumoxytol make it a uniquely versatile off-label vascular MRI contrast agent. Because of its stable intravascular distribution and high magnetic relaxivity, ferumoxytol supports high-resolution, steady-state imaging of thoracic, cardiac, and abdominal vessels.

The purpose of our pilot study was to perform a preliminary comparison of the diagnostic accuracy of ferumoxytol-enhanced MR angiography to contrast-enhanced CT angiography in the assessment of pulmonary AVMs in patients with HHT.

Abbreviations

AVM = arteriovenous malformation, GBCA = gadolinium-based contrast agent, HHT = hereditary hemorrhagic telangiectasia

Summary

Initial results suggest that ferumoxytol-enhanced MRI is a feasible alternative to CT for pulmonary arteriovenous malformation detection in hereditary hemorrhagic telangiectasia, while avoiding repeated exposure to radiation, nephrotoxic contrast material, or gadolinium-based contrast agents.

Key Points

- Arteriovenous malformations with a feeding diameter of greater than 2 mm (n = 21) were detected with MRI and CT (n = 19), MRI only (n = 2), and CT only (n = 0).
- Arteriovenous malformations with a feeding diameter of less than or equal to 2 mm (n = 22) were detected with MRI and CT (n = 16), CT only (n = 6), and MRI only (n = 0).
- No significant difference was found between CT and MRI in arteriovenous malformation size and feeding artery and draining vein diameter (P >.05).

Materials and Methods

Study Population

This study was approved for prospective data collection and retrospective review by the local institutional review board. This study was compliant with the Health Insurance Portability and Accountability Act (HIPAA). A full waiver of HIPAA authorization was obtained for retrospective review. All patients or legal guardians provided written informed consent for the contrast-enhanced MR angiography study and inclusion into our research protocol. Our study was a cross-sectional, single-center, retrospective study based on a review of prospectively collected data. This research was supported by funding from the UCLA Radiological Sciences Exploratory Research Program.

Eligibility criteria included adult patients with HHT, referred for vascular assessment with contrast-enhanced MR angiography, with available chest CT angiographic images obtained within the prior 12 months. Patients were identified and referred from the HHT clinic based on eligibility and desire to participate in the study. Retrospective analysis was performed for 10 adult patients with HHT (two men, eight women; mean age, 58.8 years; age range, 42–81 years). All patients underwent imaging at 3.0 T. The scans were performed between December 2016 and June 2017. Hemoglobin and creatinine level values obtained prior to the MRI scan were recorded (Table 1). Clinical indications for vascular evaluation were the assessment of native pulmonary AVMs, pretreatment planning for high-risk AVM embolization, and evaluation of previously treated AVMs. All patients were asymptomatic from pulmonary AVMs at the time of the study.

Exclusion criteria for this study were any contraindications to MRI scanning, hypersensitivity to iron or iron-related compounds, history of iron overload, and history of anemia other than that related to iron deficiency. None of the referred patients were excluded.

Patient Preparation

All 10 patients were deemed capable of cooperating with breath-hold instructions and denied having claustrophobia. Continuous monitoring of heart rate, pulse oximetry, and blood pressure was employed before, during, and after the MRI scan with an MRI-compatible monitoring system (Magnitude 3159 MRI patient monitor; InVivo Research, Orlando, Fla), for a minimum of 30 minutes following infusion of ferumoxytol.

MR Image Acquisition

All MR images were obtained at 3.0 T, using a 128-channel whole-body MRI system (Magnetom Skyra or Magnetom Prisma; Siemens Medical Solutions, Malvern, Pa). Phased-array multielement surface coils were used for signal reception. Body coils were configured based on body size. Multiplanar survey images were obtained using half-Fourier acquisition single-shot turbo echo without breath holding.

The stock ferumoxytol formulation was diluted with normal saline by a factor of four to six and administered over 9 minutes outside the magnet bore, using an electronic injector (Spectris Solaris; Medrad, Warrendale, Pa) to a total dose of 4 mg per kilogram of body weight. High-spatial-resolution contrast-enhanced MR angiography was performed with a spoiled three-dimensional gradient-echo sequence (see Table 2 for technical parameters), during the steady-state distribution phase of ferumoxytol. The field of view extended from the superior aspect of the skull to the level of the thighs, acquired at two or more sequential overlapping table positions.

CT Image Acquisition

CT angiographic images were obtained with a Siemens Sensation 64 CT scanner and reformatted in axial, coronal, and sagittal views with a slice thickness of 1.5 mm. The typical parameters for chest CT angiography were collimation of 0.6 mm, pitch of 1, table feed of 2 mm per rotation, and field of view of 31 cm.

Qualitative Image Analysis for Assessment of Diagnostic Quality

Four radiologists independently reviewed the MR (S.N.K., J.P.M.) and CT (B.B.B., S.K.) images to identify candidate pulmonary AVMs. Two senior radiologists (J.P.M. and J.P.F.) performed consensus review to confirm or reject each candidate AVM as a true AVM or a false-positive lesion (eg, pulmonary nodule, atelectasis).

The criteria for defining an AVM were defined as a pulmonary nidus with enhancement similar to blood pool, with a clearly identifiable feeding artery and draining vein. For statistical analysis on a per-AVM basis, each AVM sac diameter was measured and recorded in the greatest dimension. Measurement of vessel diameter was made within 5 mm of the AVM sac.

Assessment of Image Quality and Correlation between Modalities

The systemic vessels were divided into arterial segments and venous segments for quality scoring. The arterial segments

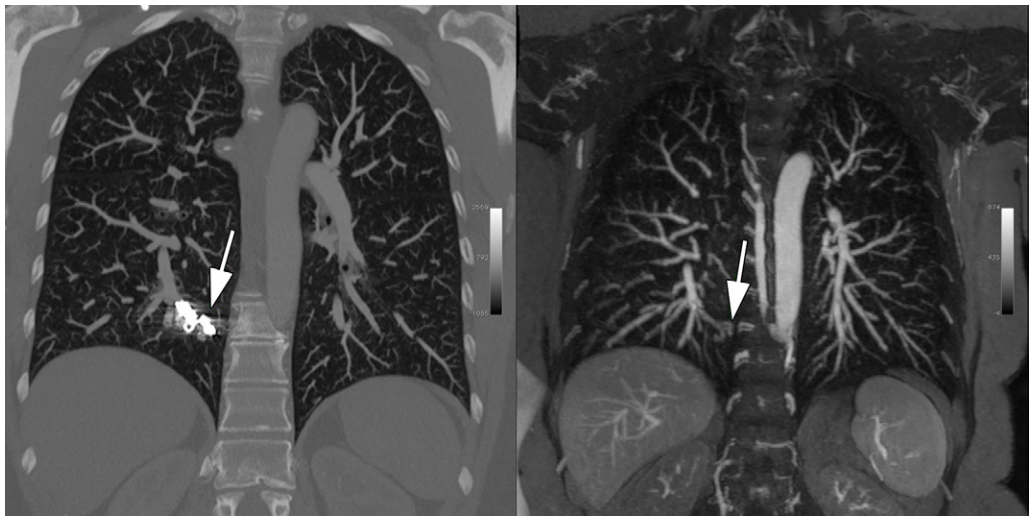

Figure 1: Coronal CT angiogram (left) in a 50-year-old woman with hereditary hemorrhagic telangectasia, who underwent prior coil embolization of a pulmonary arteriovenous malformation in the medial right lower lobe. Beam-hardening artifact related to the metallic coils (arrow in left panel) obscures the presence of recanalization that is demonstrated by the MR angiogram with ferumoxytol (arrow in right panel) and is void of beam-hardening artifact.

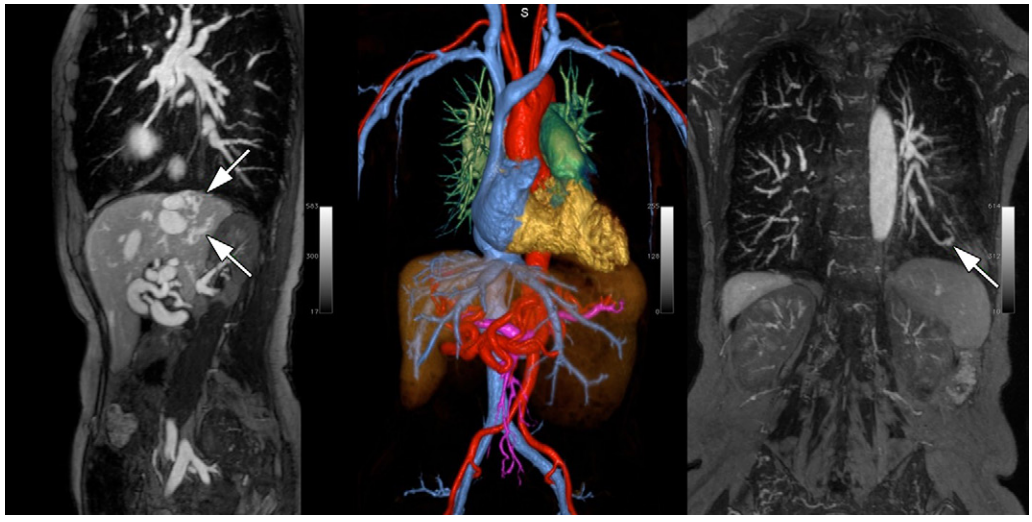

Figure 2: MR angiogram with ferumoxytol in a 58-year-old woman with hereditary hemorrhagic telangiectasia. Steady-state imaging in sagittal maximum intensity projection (MIP) view (left) demonstrates liver arteriovenous malformations (AVMs) (arrows). A pulmonary AVM is clearly visualized in the coronal MIP view in the right panel (arrow). Color three-dimensional volume rendering in the same patient (center) highlights the entire arterial and venous system and the presence of hepatic artery tortuosity and enlargement.

included the ascending aorta and arch, supra-aortic arteries, descending thoracic aorta, suprarenal abdominal aorta, and first- to fourth-order pulmonary arteries. The venous segments included the internal jugular vein, subclavian vein, innominate vein, superior vena cava, inferior vena cava, and first- to fourth-order pulmonary veins.

Image quality scoring was performed with respect to spatial resolution (0 = poor, 1 = moderate, 2 = good, 3 = excellent), contrast material bolus timing, degradation from artifacts (1 = poor, 2 = moderate, 3 = good, 4 = excellent), and artifact grade (0 = no artifacts, 1 = mild artifact not interfering with diagnostic content, 2 = moderate artifact degrading diagnostic content, 3 = severe artifact resulting in nondiagnostic images).

Statistical Analysis

Statistical analysis was performed with SPSS software (PASW 17; SPSS, Chicago, Ill). A Wilcoxon signed rank test was performed for significant differences in the image quality. A paired *t* test was performed for significant differences in AVM sac diameter, feeding artery size, and draining vein size. Comparison of CT and MRI was performed by reporting the detection rate of AVMs at both modalities, at MRI only, and at CT only. Using CT as a reference standard, decision analysis was performed to calculate sensitivity and positive predictive value of AVM detection with ferumoxytol-enhanced MRI compared with CT.

Interobserver agreement was assessed with the AC1 statistic in place of Cohen κ value, a test used in cases of greater prevalence

of positive correlation between observer agreements. The AC1 statistic is comparable to Cohen κ value and is interpreted much the same; a *P* value of < .05 was considered statistically significant. The AC1 statistic values of less than 0.20, 0.21–0.40, 0.41–0.60, 0.61–0.80, and 0.81–1.0 corresponded to poor, fair, moderate, good, and excellent agreement, respectively (Table 3).

Results

Overall Image Quality for Ferumoxytol-enhanced MRI and CT

Image quality scores were significantly higher for ferumoxytol-enhanced MRI than CT (3.87 ± 0.35 [standard deviation] vs 3.25 ± 0.46, *P* = .025).

Artifacts for Ferumoxytol-enhanced MRI and CT

Nine patients had undergone prior pulmonary AVM coil embolization. CT demonstrated the metallic coils with significant beam-hardening artifact. MR images demonstrated a signal void in the region of the coil. Two AVMs were visible only at MRI because of obscuration from coil-related artifact at CT (Fig 1).

AVM Detection

A total of 55 candidate AVMs were identified initially by the four independent observers. After secondary consensus review by the two senior radiologists, 43 of 55 AVMs were confirmed to be true AVMs (Fig 2) and 12 were rejected as alternative pathologic findings and excluded from subsequent analysis.

Of the 43 confirmed AVMs, 35 were detected at both MRI and CT, six were detected only with CT and missed with MRI, and two were detected only with MRI and missed with CT. AVMs were described as native (*n* = 13) or recanalized (*n* = 30) based on the presence of embolization coils.

Twenty-two AVMs had a feeding artery diameter of less than or equal to 2 mm; of these, 16 were detected with both ferumoxytol-enhanced MRI and CT, six were detected only with CT and missed at ferumoxytol-enhanced MRI, and zero were detected only with ferumoxytol-enhanced MRI and missed with CT. Using CT as a reference standard, the sensitivity of ferumoxytol-enhanced MRI for AVMs up to 2 mm was 72.7% (16 of 22), and the positive predictive value was 100% (16 of 16).

Twenty-one AVMs had a feeding artery diameter of greater than 2 mm (Table 4); of these, 19 were detected with both MRI and CT, two were detected only with MRI and missed with CT, and zero were detected only with CT and missed with MRI. Using CT as a reference standard, the sensitivity of ferumoxytol-enhanced MRI for AVMs greater than 2 mm was 100% (19 of 19), and the positive predictive value was 100% (19 of 19).

In subgroup analysis of previously treated AVMs, after exclusion of the AVMs that were missed at CT (*n* = 2), 28 AVMs were detected with CT and 28 AVMs were detected with MRI. The sensitivity of ferumoxytol-enhanced MRI (using CT as a reference standard) was 100% (28 of 28), and the positive predictive value was 100% (28 of 28).

Table 1: Patient Demographics

Demographic	Patients with HHT
Total in study	10
Sex	Two men, eight women
Age range (y)	42.0–81.0
Mean age (y)*	58.8 ± 11.5
Weight range (kg)	46.8–108
Mean weight (kg)*	78.1 ± 20.6
Average pre-MRI creatinine level	0.84
Average pre-MRI hemoglobin level	11.3

Note.—HHT = hereditary hemorrhagic telangiectasia.
* Data are means ± standard deviations.

Table 2: Technical Parameters

Parameter	Ferumoxytol-enhanced MRI
Repetition time (msec)	1.94–2.67
Echo time (msec)	0.81–0.96
Flip angle (degrees)	11–20
Bandwidth (Hz/pixel)	610–615
Voxel dimensions (mm^3)	1 × 1.2 × 1.3
No. of phase encoding steps	226–280
Acquisition time (sec)	16.5–20.3
Specific absorption rate (W/kg)	1.2–2.4
Integrated parallel acquisition technique factor	4

Note.—3.0-T 32-channel whole-body scanner (Magnetom TIM Trio; Siemens Medical Solution, Malvern, Pa), gradient strength = 40 mT/m, slew rate = 200 mT/m/msec.

AVM Sac Size, Feeding Artery Diameter, and Draining Vein Diameter

No significant difference was found between ferumoxytol-enhanced MRI and CT for average AVM sac diameter (MRI 4.07 mm ± 1.56, CT 4.28 mm ± 1.77; *P* = .355), average feeding artery diameter (MRI 2.13 mm ± 0.31, CT 1.91 mm ± 0.37;*P* = .447), or average draining vein diameter (MRI 2.46 mm ± 0.55, CT 2.17 mm ± 0.78; *P* = .284).

Adverse Events

No adverse events were found with the use of ferumoxytol during or immediately after the MRI scan (30-minute observation period) or following the MRI scan by retrospective chart review until the time of manuscript preparation.

Discussion

The results of our study showed that ferumoxytol-enhanced MRI at 3.0 T was technically feasible for the detection of pulmonary AVMs in patients with HHT. Ferumoxytol-enhanced

Table 3: Observer Agreement and Correlation AC1 Statistic

	Ferumoxytol-enhanced MRI		CT	
Arterial and Venous Segment	Mean Observer Score	AC1 Statistic	Mean Observer Score	AC1 Statistic
Ascending aorta/arch	3.75 ± 0.46	1.0	3.50 ± 0.55	1.0
Supra-aortic arteries	4.00 ± 0.00	1.0	3.67 ± 0.52	1.0
Descending thoracic aorta	4.00 ± 0.00	1.0	3.83 ± 0.41	1.0
Suprarenal abdominal aorta	4.00 ± 0.00	1.0	3.67 ± 0.52	1.0
First-order pulmonary artery	4.00 ± 0.00	1.0	3.38 ± 0.52	1.0
Second-order pulmonary artery branches	4.00 ± 0.00	1.0	3.38 ± 0.52	1.0
Third-order pulmonary artery branches	4.00 ± 0.00	1.0	3.38 ± 0.52	1.0
Fourth-order pulmonary artery branches	3.75 ± 0.46	1.0	3.38 ± 0.52	1.0
Internal jugular vein	4.00 ± 0.00	1.0	Not assessable	Not assessable
Subclavian vein	4.00 ± 0.00	1.0	Not assessable	Not assessable
Innominate vein	4.00 ± 0.00	1.0	Not assessable	Not assessable
Superior vena cava	4.00 ± 0.00	1.0	Not assessable	Not assessable
Inferior vena cava	4.00 ± 0.00	1.0	Not assessable	Not assessable
First-order pulmonary veins	4.00 ± 0.00	1.0	3.38 ± 0.52	1.0
Second-order pulmonary vein tributaries	4.00 ± 0.00	1.0	3.25 ± 0.46	1.0
Third-order pulmonary vein tributaries	4.00 ± 0.00	1.0	3.38 ± 0.52	1.0
Fourth-order pulmonary vein tributaries	3.88 ± 0.35	1.0	3.38 ± 0.52	1.0

Note.—Unless otherwise indicated, data are means ± standard deviations.

Table 4: Distribution of AVMs per Patient with HHT

Patient with HHT	AVM Feeding Artery < 2 mm	AVM Feeding Artery > 2 mm
1	0	2
2	3	1
3	1	0
4	3	5
5	3	1
6	0	1
7	3	2
8	0	2
9	3	12
10	1	0

Note.—AVM = arteriovenous malformation, HHT = hereditary hemorrhagic telangiectasia.

MR angiography produced high-resolution, diagnostic quality images safely and consistently in all patients.

Our study found that when considering all AVMs with a feeding artery diameter ranging from 1.2 to 5.4 mm, 35 were detected with both MRI and CT, six were detected only with CT and missed with MRI, and two were detected only with MRI and missed with CT. The sensitivity of ferumoxytol-enhanced MRI was 85.4% (35 of 41), and the positive predictive value was 100% (35 of 35). The AVMs missed at CT were generally the result of obscuration from significant beam-hardening artifact related to embolization coils. The AVMs missed at MRI were the result of small size (< 2 mm) and limitation of spatial resolution. When only the AVMs with a feeding artery diameter of greater than 2 mm were considered (n = 22), all AVMs were detected at MRI and two were missed at CT because of beam-hardening artifact. Although practice patterns vary, AVMs with a feeding artery size of less than 2 mm have traditionally not been indicated for treatment because of a low risk of complications in these patients (4,13). In our cohort of 43 pulmonary AVMs, ferumoxytol-enhanced MRI detected all AVMs 2 mm or larger, and MRI may be superior to CT at detecting recanalization of pulmonary AVMs in the presence of embolization coils.

Another advantage of ferumoxytol-enhanced MRI was that simultaneous evaluation for pulmonary, cerebral, and hepatic AVMs was possible all within one scan, following a single contrast material injection. This was an important advantage for patients with HHT who frequently require separate imaging studies to screen for AVMs in different locations.

Prior studies suggest that ferumoxytol is comparable to standard GBCAs for contrast-enhanced MR angiography (14,15), and ferumoxytol provides the added benefit of iron supplementation, which is relevant in patients with chronic bleeding.

Indeed, all of our patients with HHT were anemic (hemoglobin level < 12.0 g/dL) because of blood loss from nasal and gastrointestinal telangiectasias, supporting the value of ferumoxytol as a theranostic agent in this population.

Ferumoxytol addresses several of the safety concerns raised concerning GBCAs. Beyond the well-established association between certain GBCAs and nephrogenic systemic fibrosis in patients with renal failure, the phenomenon of gadolinium brain deposition is the subject of intense discussion and research (16).

Another safety concern relates to the cumulative radiation exposure inherent in repeated CT scanning. Because CT is currently the standard of reference examination for detection of pulmonary AVMs, the recommendation is to perform screenings at intervals of 3 to 5 years throughout the lifetime of a patient with HHT, particularly in patients with previously treated AVMs or with a positive bubble study. When using MRI as an alternate imaging modality, many of these scans could be avoided.

Several limitations were present in our study. First, the sample size was small in this pilot study. Second, because of the study's retrospective nature, the CT and ferumoxytol-enhanced MR images were temporally separated by weeks to months in many cases, rather than being obtained the same day. Third, within-patient correlation of pulmonary AVMs was not addressed in the current analysis, which may have affected the results in this study because it was unknown if the missed AVMs were attributable to modality or patient factors.

In conclusion, our initial results suggested that ferumoxytol-enhanced MR angiography showed promise as a powerful and reliable diagnostic tool for lung AVM screening in patients with HHT. It provided a feasible alternative to CT, while avoiding exposure to radiation, nephrotoxic contrast material, and gadolinium.

Acknowledgment: James Sayre for statistical analysis.

Author contributions: Guarantors of integrity of entire study, J.P.M., S.K., J.P.F.; study concepts/study design or data acquisition or data analysis/interpretation, all authors; manuscript drafting or manuscript revision for important intellectual content, all authors; approval of final version of submitted manuscript, all authors; agrees to ensure any questions related to the work are appropriately resolved, all authors; literature research, S.N.K., J.P.F.; clinical studies, J.P.M., B.B.B., J.P.F.; experimental studies, J.P.M., B.B.B.; and manuscript editing, S.N.K., J.P.M., S.K., J.P.F.

Disclosures of Conflicts of Interest: **S.N.K.** disclosed no relevant relationships. **J.P.M.** disclosed no relevant relationships. **B.B.B.** disclosed no relevant relationships. **S.K.** disclosed no relevant relationships. **J.P.F.** disclosed no relevant relationships

References

1. Guttmacher AE, Marchuk DA, White RI Jr. Hereditary hemorrhagic telangectasia. N Engl J Med 1995;333(14):918–924.
2. Fuchizaki U, Miyamori H, Kitagawa S, Kaneko S, Kobayashi K. Hereditary haemorrhagic telangiectasia (Rendu-Osler-Weber disease). Lancet 2003;362(9394):1490–1494.
3. Cottin V, Chinet T, Lavolé A, et al. Pulmonary arteriovenous malformations in hereditary hemorrhagic telangiectasia: a series of 126 patients. Medicine (Baltimore) 2007;86(1):1–17.
4. Faughnan ME, Palda VA, Garcia-Tsao G, et al. International guidelines for the diagnosis and management of hereditary haemorrhagic telangiectasia. J Med Genet 2011;48(2):73–87.
5. McDonald J, Bayrak-Toydemir P, Pyeritz RE. Hereditary hemorrhagic telangiectasia: an overview of diagnosis, management, and pathogenesis. Genet Med 2011;13(7):607–616.
6. Pierucci P, Murphy J, Henderson KJ, Chyun DA, White RI Jr. New definition and natural history of patients with diffuse pulmonary arteriovenous malformations: twenty-seven-year experience. Chest 2008;133(3):653–661.
7. Faughnan ME, Lui YW, Wirth JA, et al. Diffuse pulmonary arteriovenous malformations: characteristics and prognosis. Chest 2000;117(1):31–38.
8. Finn JP, Nguyen KL, Han F, et al. Cardiovascular MRI with ferumoxytol. Clin Radiol 2016;71(8):796–806.
9. Nguyen KL, Yoshida T, Han F, et al. MRI with ferumoxytol: A single center experience of safety across the age spectrum. J Magn Reson Imaging 2017;45(3):804–812.
10. Han F, Rapacchi S, Khan S, et al. Four-dimensional, multiphase, steady-state imaging with contrast enhancement (MUSIC) in the heart: a feasibility study in children. Magn Reson Med 2015;74(4):1042–1049.
11. Toth GB, Varallyay CG, Horvath A, et al. Current and potential imaging applications of ferumoxytol for magnetic resonance imaging. Kidney Int 2017;92(1):47–66.
12. Nayak AB, Luhar A, Hanudel M, et al. High-resolution, whole-body vascular imaging with ferumoxytol as an alternative to gadolinium agents in a pediatric chronic kidney disease cohort. Pediatr Nephrol 2015;30(3):515–521.
13. Trerotola SO, Pyeritz RE, White RI Jr, et al. 2009 Treatment guidelines for hereditary hemorrhagic telangiectasia. J Vasc Interv Radiol 2010;21(2):179.
14. Prince MR, Zhang HL, Chabra SG, Jacobs P, Wang Y. A pilot investigation of new superparamagnetic iron oxide (ferumoxytol) as a contrast agent for cardiovascular MRI. J XRay Sci Technol 2003;11(4):231–240.
15. Li W, Tutton S, Vu AT, et al. First-pass contrast-enhanced magnetic resonance angiography in humans using ferumoxytol, a novel ultrasmall superparamagnetic iron oxide (USPIO)-based blood pool agent. J Magn Reson Imaging 2005;21(1):46–52.
16. Gulani V, Calamante F, Shellock FG, Kanal E, Reeder SB; International Society for Magnetic Resonance in Medicine. Gadolinium deposition in the brain: summary of evidence and recommendations. Lancet Neurol 2017;16(7):564–570.